Optical and Quantum Electronics (2023) 55:926
https://doi.org/10.1007/s11082-023-05185-x

Design of a multilayer wideband absorber based on frequency selective surface

Maojun Li[1] · **Wei Zhang**[1]

Received: 22 May 2023 / Accepted: 12 July 2023 / Published online: 7 August 2023

Abstract
This paper presents a broadband absorber consisting of three frequency selective surfaces (FSS) layers. The FSS layers consist of four identical rectangles and two circular arcs, a prototype is fabricated, and measurements are performed in an anechoic chamber to validate the proposed design method. The consistency of the simulation and measurement results verifies the analysis and design principle. The simulation results show that the absorption of the proposed absorber is greater than 80% in the frequency range of 3.8–11.9 GHz, while the relative absorption bandwidth is 103%. Meanwhile, the absorption of TE and TM waves hardly changes when the incident angle rises to 25°.

Keywords Absorb · Broadband · Frequency selective surface · Multilayer

1 Introduction

As a result of the rapid development of radar detection technology and mobile communication, the requirements for wave-absorbing materials are becoming higher and higher. The conventional absorbing material Salisbury screen (Johnson et al. 2012) consists of a metal-backed impedance layer, a space layer and a grounding plate. The Salisbury screen exhibits a straightforward configuration; however, it possesses a limited absorption bandwidth, making it less suitable for practical engineering applications. Jaumann absorber (Chen et al. 2004; Smith et al. 2000) is a modification of Salisbury screen, which is the absorber is constructed using multiple layers of dielectric and impedance materials. While the absorber achieves a significant improvement in absorption bandwidth, the overall thickness of its structure is increased and the difficulty and complexity of its structural design increase accordingly, thus limiting its application in practice.

With advent of time, researchers have found that using magnetic patterns as FSS layers can broaden the absorption bandwidth by increasing the magnetic loss of the absorber, but the poor thermal stability of general magnetic materials can lead to unstable absorption

✉ Wei Zhang
zhang_wei@nwu.edu.cn

Maojun Li
lmj1515@163.com

[1] School of Information Science and Technology, Northwest University, Xi'an 710127, China

performances (Landy et al. 2009; Liu et al. 2017). In the light of this, to overcome the shortcomings of the previously designed absorbers and to design absorbers with a wide band and small size, absorbers utilizing frequency selective surfaces (FSS) have garnered significant attention in academic research. (Landy et al. 2019), using a traditional "sandwich" structure—metal resonant structure, dielectric layer, and metal backplane. The absorber demonstrates an absorption rate exceeding 98% at 11.4 GHz. Sabah C et al. designed a ring and cross-line based absorber, which can achieve perfect absorption at 2.76 GHz with 99.9% absorption (Alù and Engheta 2005). Li et al. designed and fabricated a dual frequency absorber. Ning, Renxia et al. designed a tunable absorber with three independently tunable operating bands in the C and X band range, 6.36 GHz, 7.96–10.12 (GHz), with absorption rates of 93%, 99%, and 99%, respectively, using mutual coupling between resonators, and the absorber can still maintain high absorption efficiency at these frequency points at oblique incidence (Zhao et al. 2014).

With the continuous development of radio technology and communication field, the function requirements of the absorber also gradually become more and more, simply in one or more frequency points to achieve the effect of absorption has not been able to meet the actual demand. Many scholars at home and abroad have been carrying out research on broadband absorbers. In 2010, a single-layer broadband FSS with a relative bandwidth of 20 dB to 36.5% has been achieved (Shen et al. 2013). compared to a single-layer FSS structure, a wider band absorption can be attained by using a multilayer design, F. Ding devised a multilayer stacked pyramid structure (Ding et al. 2012), which can realize a relative bandwidth of 61.3%, Chen et al. made the absorption performance at the resonant frequency point enhanced by the operation of superimposing multilayer metal structures to achieve the expected broadband absorption effect (Xu et al. 2017).In their study, Li et al. introduced a novel technique by combining two resonant rings with varying sizes on top of a dielectric layer, resulting in a total absorber thickness of 3.6 mm. This ingenious design achieved an impressive absorption rate of 80% within 5.34–14.72 (GHz). Notably, this absorber also exhibited remarkable absorption performance even when subjected to oblique incidences of up to 30° (Cao et al. 2017). Successively, SOME other multilayer designs with 65–101% bandwidth have also been proposed (Wu et al. 2019; Yang et al. 2013; Chen et al. 2018; Wang and Zhang 2016; Dong et al. 2016); however, the bandwidth can be further improved.

With these considerations in mind, this work proposes a multilayer broadband frequency-selective surface, a structure that achieves perfect microwave absorption in 3.8–11.9 (GHz), while being insensitive to polarization and electromagnetic wave incidence angle. The presented structure has also been built and its measured response agrees well with the computer results.

2 Design and simulation

2.1 Absorber structure

The broadband frequency selective surface absorber cell is shown in Fig. 1a. The entire composition is composed of three FSS metal layers, a metal backplane and a matching layer, and three dielectric layers. PTFE with a refractive index of 1.35 was selected as the matching layer, and despite the available options, the choice was made to utilize an FR4 plate as the dielectric coating. The FR4 plate possesses a relative permittivity of 4.4 and a

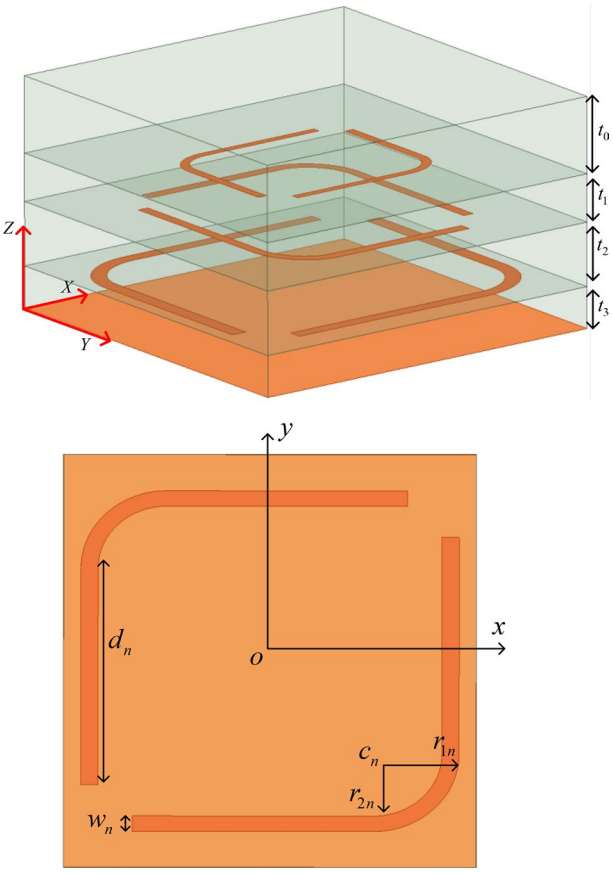

Fig. 1 FSS structure **a** three-dimensional view of FSS unit cell **b** schematic structure of the FSS unit cell

loss angle tangent of 0.02.The frequency selective surface (FSS) layers and metallic ground plate are fabricated using copper material, which possesses a conductivity of $5.8 \times 10^7 \mathrm{S/m}$ and a thickness of 0.02 mm.With the center of the structure as the origin to establish the coordinate system, the FSS surface is made up of two circles and four identical rectangles with circular arc position c_n, large circle radius r_{1n}, small circle radius r_{2n} and width w_n. The downscales n are intended to differentiate between the three distinct dimensional units.

The optimal absorber geometrical parameters are as follows in Table 1.

The performance analysis of the wave absorber was conducted using HFSS through a series of simulation experiments. These simulations employed unit cell boundary conditions in the x and y directions, while the Floquet port condition was utilized in the z direction. In order to assess the effectiveness of the absorber, the absorptivity (referred to as $A = 1 - |S_{11}|^2 - |S_{21}|^2$) was determined by calculating the product of the reflection coefficient (S_{11}) and the transmission coefficient (S_{21}) of the unit structure. However, in this particular scenario, the presence of a copper flooring rendered the transmission coefficient S_{21} negligible, resulting in a value that approached zero. Consequently, the absorptivity of the structure was determined solely by the reflection coefficient S_{11}. To quantify the absorber's performance, the absorptivity was calculated as $A = 1 - |S_{11}|^2$. Figure 2a illustrates the absorption characteristics of the frequency selective surfaces (FSS) when illuminated by

Table 1 Physical dimensions the elementary cell

p	t_0	t_1	t_2	t_3	d_1	d_2
12	2.8	1.5	2	0.7	4.2	5.6
w_2	w_3	r_{11}	r_{12}	r_{21}	r_{13}	r_{23}
0.35	0.45	1.5	2	1.2	2.5	2
c_1	c_2	c_3	w_1	d_3	r_{22}	
(−1.8, 1.5)	(−2.4, −2.1)	(3, −2.7)	0.25	6.3	1.6	

Note: All dimensions are in mm

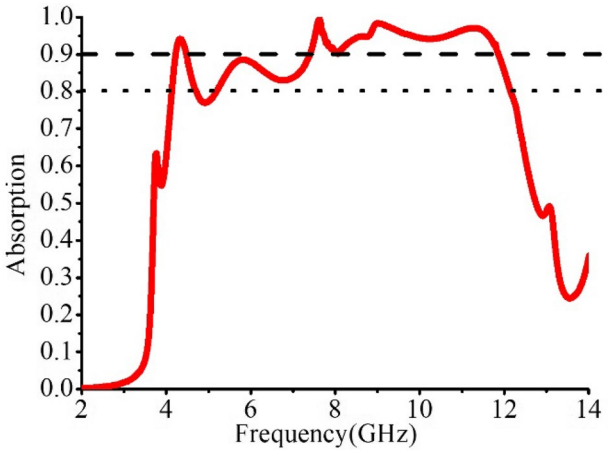

Fig. 2 Absorption rate

normal incident waves. It is observed that within 3.8–11.9 (GHz), the suggested absorber exhibits an absorption rate exceeding 80%. Additionally, the absorber demonstrates a relative absorption bandwidth of 103%, indicating its ability to effectively absorb a wide range of frequencies.

Wideband absorbers have to be studied for the stability of incident electromagnetic wave polarization and incident angle. The absorption characteristics of TE and TM waves at different incidence angles are considered respectively. As depicted in Fig. 3, one can observe a noticeable trend wherein the absorption bandwidth gradually diminishes as the incident angle rises within 3.8–11.9 (GHz). This phenomenon can be attributed to the underlying principles of destructive interference upon which the broadband absorber relies. With an increase in the incident angle, the effective pathway traversed by electromagnetic waves through the absorber also increases, leading to alterations in the phase difference. Consequently, this disruption in phase matching impairs the absorber's ability to efficiently absorb electromagnetic energy, thereby adversely impacting its absorption performance.

2.2 Principle of operation

Reflection, transmission, absorption and refraction can occur when the electromagnetic wave incident on the frequency selection surface, and the energy conservation law is followed. In order to ensure the matching between the absorber and the air layer, PTFE with

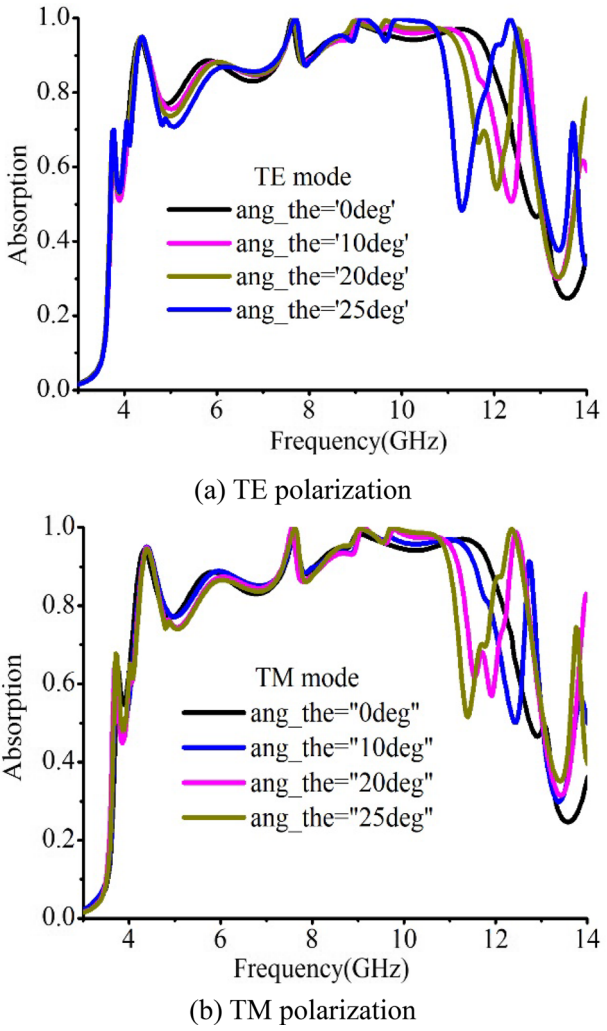

Fig. 3 The absorption characteristics of the designed structure were investigated for both normal and oblique angles of incidence, considering waves with TE and TM

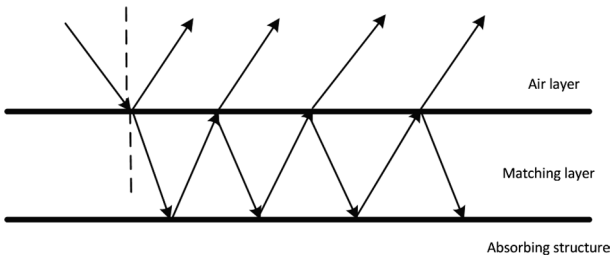

Fig. 4 The absorption characteristics of the designed structure are evaluated for both normal and oblique angles of incidence, considering waves polarized in the TE TM

refractive index of 1.35 is selected as the matching layer in this design. The Fig. 4 illustrates the transmission properties of electromagnetic waves within the matching layer.

When the phase discrepancy between the reflected waves, which transpire at the two interfaces, attains half a wavelength, it necessitates the effective distance traveled by the

electromagnetic wave within the matching layer to be precisely one quarter of the wavelength. The characteristic wavelength of the electromagnetic wave in the matching layer, denoted as λ_{AR}, can be determined by the interplay of the matching layer's thickness t and its refractive index n (Shelby et al. 2001):

$$n \cdot t = \frac{m \cdot \lambda_{AR}}{4} \tag{1}$$

where C represents the velocity of light in a vacuum, while m denotes a positive integer that is odd in value.

When the electromagnetic wave is incident vertically to the absorber, as the thickness of the matching layer increases, the absorption curve of the absorber is depicted in Fig. 5.

It can be observed through Fig. 3d that as the thickness of the matching layer increases, the absorption peaks at some frequency points show an upper shift phenomenon, which is commonly called "Redshift". This is because the absorption peaks in this frequency band are formed due to the phase extinction of electromagnetic interference, so it also verifies Eq. (1).

In this design, each dielectric layer and the FSS above it form a dielectric layer. The different thicknesses of the three dielectric layers can modify the refractive index of the whole absorber and adjust the phase of the electromagnetic waves entering the absorber. To further clarify the destructive interference mechanisms, the transmission enhancement characteristics of the multilayer absorber are discussed. Neglecting the thickness of the copper layer of the intermediate metal unit, Fig. 6 illustrates the transmission model depicting the arrangement of the multilayer absorber.

In order to simplify the structure, the three metal cells and the FR4 layer are regarded as equivalent dielectric layer 1, and the metallic copper backplane is replaced by equivalent dielectric layer 2; as demonstrated in the Fig. 7. The cumulative reflection of the entire system is the combined effect of the reflections occurring at the two interfaces (Shelby et al. 2001).

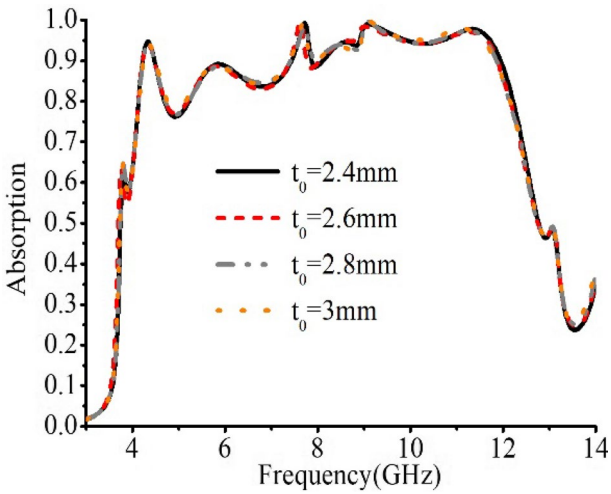

Fig. 5 Absorption curves of absorbers with different top layer thicknesses t_0

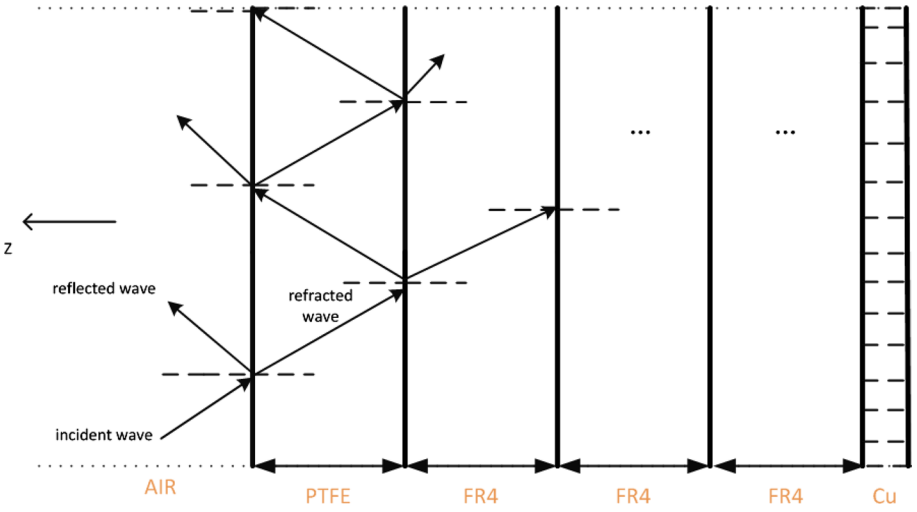

Fig. 6 Transmission model for multilayer absorbers

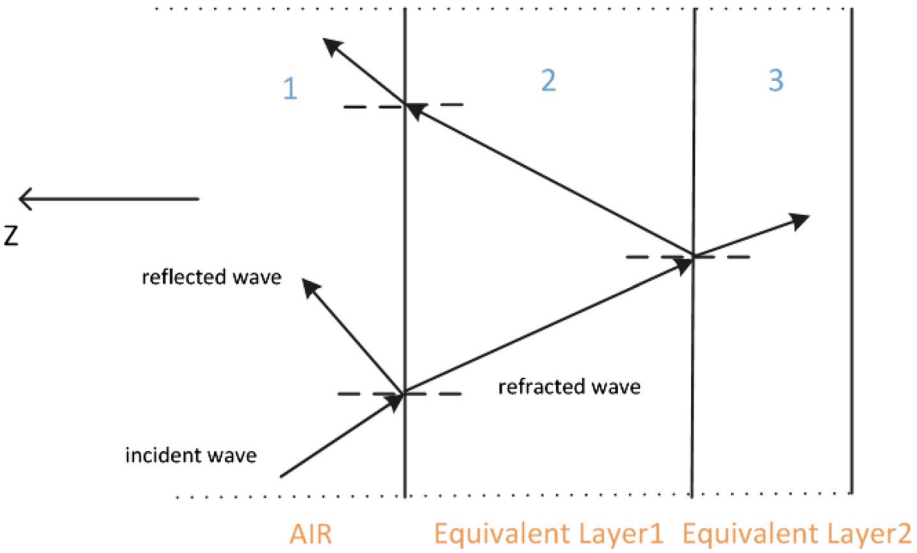

Fig. 7 Simplified transmission model

$$\tilde{r} = \frac{R_{12}\exp\left(j\phi_{12}\right) + T_{12}R_{23}T_{21}(j\zeta)}{1 - R_{21}R_{23}\exp\left[j\left(\phi_{12} + \phi_{23} + 2\beta\right)\right]} \tag{2}$$

$$\tilde{t} = \frac{T_{12}T_{23}\exp\left[j\left(\psi_{12} + \psi_{23} + \zeta\right)\right]}{1 - R_{21}R_{23}\exp\left[j\left(\phi_{12} + \phi_{23} + 2\beta\right)\right]} \tag{3}$$

The variable ϕ_{12} symbolizes the phase alteration triggered by the reflection transpiring at the boundary shared by air (designated as 1) and the corresponding medium (designated as 2). Similarly, ϕ_{23} represents a similar phase variation. Moreover, ψ_{12} signifies the phase shift brought about through the transition of electromagnetic waves from medium 1 (air) to the equivalent medium 2, while ψ_{23} corresponds to a similar phase shift. The coefficients R_{12}, R_{23}, T_{12}, T_{23} denote the amplitudes of the Fresnel coefficients governing the interaction between these two interfaces. These coefficients possess two crucial properties: they are all positive real numbers and satisfy the following equation.

$$\zeta = \psi_{12} + \phi_{23} + \psi_{23} + 2\beta \tag{4}$$

The wave vector in an unobstructed space is denoted as $\beta = -nk_0t/\cos\alpha_2$, while k_0 represents another wave vector in an unobstructed space. The refractive index (RI) of the equivalent dielectric layer is represented by n. Consequently, the reflection of the entire system can be mathematically represented as follows:

$$R = |\tilde{r}|^2 = \frac{R_{12}^2 + (T_{12}R_{23}T_{21})^2 + 2R_{12}T_{12}R_{23}T_{21}\cos\left(\phi_{12} - \zeta\right)}{1 + \left(R_{23}R_{21}\right)^2 - 2\cos\left(\phi_{12} + \phi_{23} + 2\beta\right)R_{23}R_{21}} \tag{5}$$

$\phi_{12} - \zeta$ represents the accumulated phase shifts caused by the reflections that take place at the two interfaces. Due to the high refractive index (RI) value of the material, the wave at the second interface experiences near-total reflection ($R_{23} \approx 1$). Assuming the following conditions are met:

$$R_{12} \approx T_{12} \cdot T_{21} \tag{6}$$

$$\phi_{23} - \zeta = (2N + 1)\pi \tag{7}$$

Then, Eq. (5) could be optimized as

$$R = |\tilde{r}|^2 = \frac{R_{12}^2 + (T_{12}T_{21})^2 - 2R_{12}T_{12}T_{21}}{1 + \left(R_{23}R_{21}\right)^2 - 2\cos\left(\phi_{12} + \phi_{23} + 2\beta\right)R_{23}R_{21}} \tag{8}$$

By reasonably tuning the values of R_{12}, T_{12} and T_{21} to satisfy Eq. (5), the electromagnetic wave interference phase extinction condition is realized. The frequency points where the "Redshift" phenomenon appears in Fig. 5 are based on this mechanism. Yet, the absorption frequencies and peaks at 3.8, 13.1, 14.7 (GHz) barely change with the addition of the matching layer, due to the fact that these three absorption peaks are caused by the electromagnetic resonance.

Figure 8 presents a comprehensive overview of the electric field strength, magnetic field strength, and distribution of surface current within the absorber, specifically at 3.8 GHz. The findings from this analysis indicate that, at this particular frequency, the surface current predominantly concentrates on the FSS (Frequency Selective Surface) structure situated in the bottommost layer of the absorber. Notably, at 3.8 GHz, the surface current primarily resides within the lowest metallic FSS layer, with two distinct electrodes being stimulated at the initiation and termination points of the current flow. These regions of electrode excitation coincide with the central hubs of electric field energy concentration. Furthermore, the areas displaying the strongest intensity of

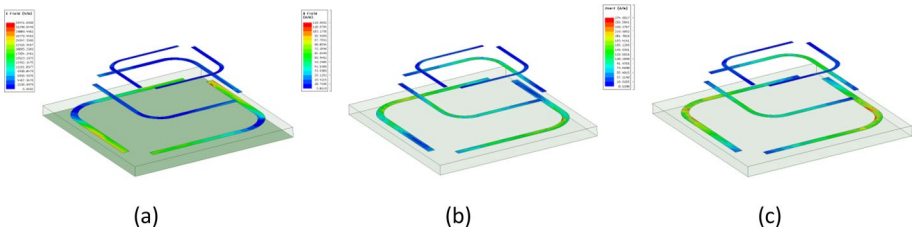

Fig. 8 showcases the spatial allocation of field characteristics at 3.8 GHz

current are characterized by the emergence of two magnetic poles, where the magnetic field energy is notably focused. This results in an electromagnetic resonance at 3.8 GHz, resulting in the absorption of electromagnetic wave energy.

Similarly, the spatial arrangement of the absorbing material is examined at 13.1 and 14.7 (GHz), as illustrated in Figs. 9 and 10, respectively. The resonance principle is similar to that of 3.8 GHz, with the difference that the surface currents at 13.1 GHz are mainly concentrated at the metal FSS in the middle layer, and at 14.7 GHz at the uppermost metal FSS. Upon careful examination of Figs. 8, 9, and 10, it becomes evident that the prominent peaks observed at these specific frequencies can be attributed to the magnetic response loss. It is noteworthy that these peaks do not arise from the principle of interference phase extinction, as initially hypothesized.

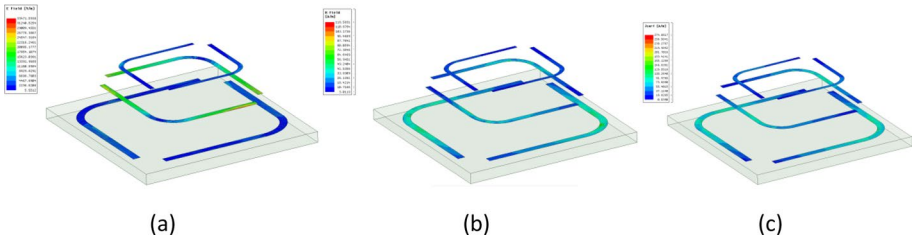

Fig. 9 Field distribution at 13.1 GHz **a** electric field intensity distribution of the absorber **b** magnetic field intensity distribution of the absorber **c** surface current distribution of wave absorber

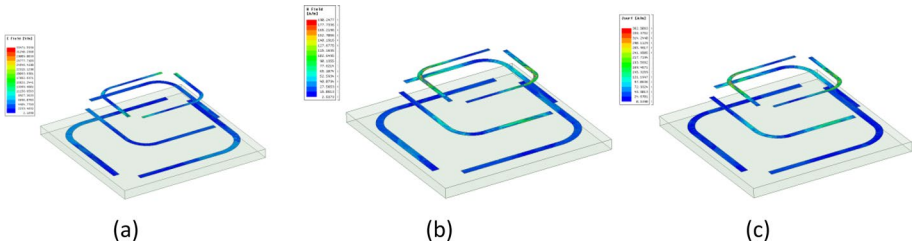

Fig. 10 At 14.7 GHz, the following field distributions are observed in the absorber

3 Measurement setup

The spatial wave test method was adopted for testing and verification. The sample and test of broadband absorbers are shown in Fig. 11. By employing a configuration that involves multiple conventional horn antennas coupled to a vector network analyzer, a comprehensive testing procedure was conducted across distinct frequency bands. The obtained outcomes are visually presented in Fig. 12. Upon careful observation, it becomes apparent that

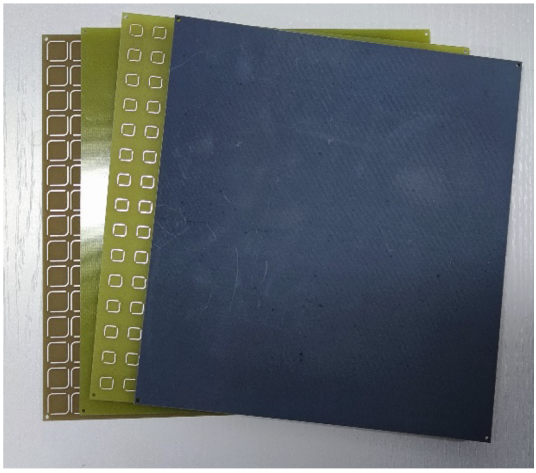

a. The proposed FSS prototypes

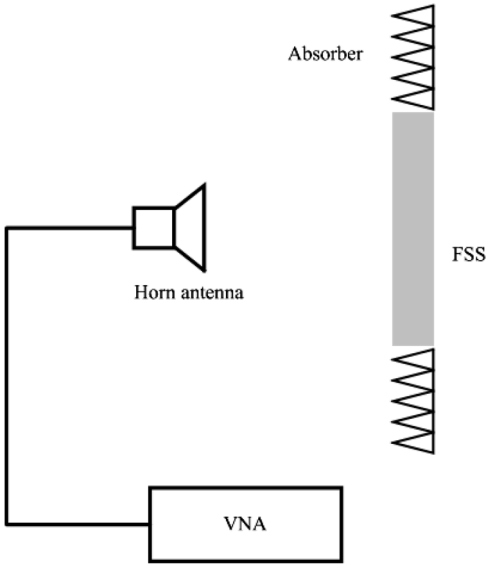

b. Block diagram

Fig. 11 Experimental system and the proposed FSS prototypes

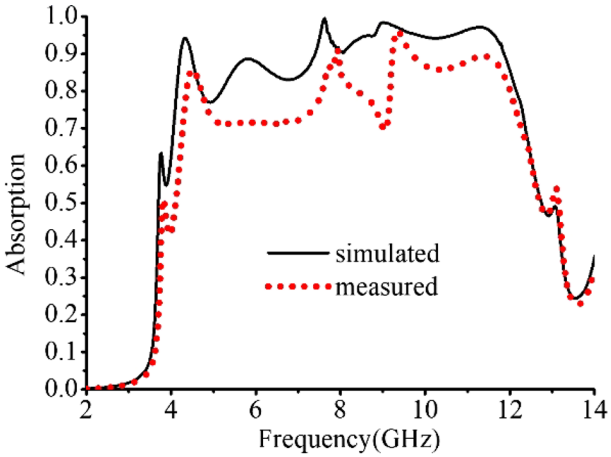

Fig. 12 Measured reflection coefficients of FSS

due to inherent factors such as inevitable processing errors and various other perturbations, the actual absorption effect exhibited by the sample under investigation falls slightly short in comparison to the anticipated results projected by the simulation.

4 Conclusion

In summary, we put forward a broadband absorber based on the destructive interference mechanisms, through the principle analysis and practical measurements, it is proved that it is truly designed based on the interferometric phase extinction theory, while the utilization of electromagnetic waves in 3.8–11.9 (GHz) exhibits exceptional absorption efficiency, reaching as high as 80%. Moreover, the relative range of frequencies absorbed spans 103% of the given frequency range. When the angle of incidence increases to 25°, there is minimal change in the absorption of both TE and TM waves. It can be extensively implemented in microwave stealth technology.

Authors' contributions ML, School of Information Science and Technology, Northwest University, Xi'an, CO 710127, China; drafted or revised the manuscript. ML will be available throughout the submission and peer review process to respond to editorial queries in a timely way, and should be available after publication to respond to critiques of the work and cooperate with any requests from the journal for data or additional information should questions about the paper arise after publication. WZ, School of Information Science and Technology, Northwest University, Xi'an, CO 710127, China; Conceived and designed the work that led to the submission, acquired data, and played an important role in interpreting the results.Project administration management and coordination responsibility for the research activity planning and execution.

Data sharing agreement No dataset was generated or analyzed during this study.

Funding This work was supported by the National Natural Science Foundation of China (No.62001384); Natural Science Basic Research Plan in Shaanxi Province of China (No. 2020JQ-605); and the China Postdoctoral Science Foundation (No.2020M683694XB).

Declarations

Conflict of interest All authors disclosed no relevant relationships.

Ethical approval The paper did not involve animal or human studies and did not require an rthical approval.

References

Alù, A., Engheta, N.: Achieving transparency with plasmonic and metamaterial coatings. Phys. Rev. E **72**(1), 166 (2005). https://doi.org/10.1103/PhysRevE.72.016623

Cao, X., Zhang, Y., Li, L., Zhao, Z.: A compact and broadband absorber with fractal Hilbert-shaped structure for the microwave regime. Microw. Opt. Technol. Lett. **59**(4), 760–764 (2017)

Chen, X., Grzegorczyk, T.M., Wu, B.I., Pacheco, J., Kong, J.A.: Robust method to retrieve the constitutive effective parameters of metamaterials. Phys. Rev. E **70**(1), 016608 (2004). https://doi.org/10.1103/PhysRevE.70.016608

Chen H., Yang X., Wu S., Zhang D., Xiao H., Huang K., Zhu Z., Yuan J.: Flexible and conformable broadband metamaterial absorber with wide-angle and polarization stability for radar application. Materials Research Express. **5**(1), 015804 (2018). https://doi.org/10.1088/2053-1591/aaa7ab

Ding F., Cui Y., Ge X., Jin Y., He S.: Ultra-broadband microwave metamaterial absorber. Applied Physics Letters, **100**(10):103506–103506–4. (2012). https://doi.org/10.1063/1.3692178

Dong, P., Yang, M., Wang, W., Li, Y., Cui, T.J.: Wide-angle and polarization-independent metamaterial absorber based on fractal structures. J. Appl. Phys. **120**(4), 105 (2016)

Johnson, A.R., Thompson, B.R., Roberts, D.A., Williams, C.M.: Tunable metamaterial absorber for infrared frequencies. Opt. Express **20**(4), 3556–3561 (2012)

Landy, N.I., Bingham, C.M., Tyler, T., Smith, D.R.: Design, theory, and measurement of a polarization-insensitive absorber for terahertz imaging. Phys. Rev. B **79**(12), 125 (2009). https://doi.org/10.1103/PhysRevB.79.125104

Li, S., Zhang, F., Yang, M., Qu, S.: Broadband polarization-insensitive and wide-angle absorption using a tunable metasurface with an embedded graphene layer. Appl. Opt. **57**(4), 259–263 (2018)

Liu, X., Guo, L., Shi, X., Li, Y., Wang, H.: A novel wideband polarization-insensitive metamaterial absorber based on perfect impedance matching. Opt. Express **25**(9), 302–311 (2017)

Shen, X., Cui, T.J., Zhao, J., Ma, H.F.: Polarization-independent wide-angle triple-band metamaterial absorber. Opt. Express **21**(22), 152–160 (2013)

Shelby R.A., Smith D.R., Schultz S.: Experimental Verification of a Negative Index of Refraction. Science. **292**(5514): 77–79 (2001) https://doi.org/10.1126/science.1058847

Smith, D.R., Padilla, W.J., Vier, D.C., Nemat-Nasser, S.C., Schultz, S.: Composite medium with simultaneously negative permeability and permittivity. Phys. Rev. Lett. **84**(18), 4184–4187 (2000)

Wang, H., Zhang, B.: Tunable wide-angle perfect absorber based on phase-change materials. Opt. Express **24**(15), 166–167 (2016)

Wu, B., Ye, X., Yuan, B., Zhu, B.: Polarization-insensitive and wide-angle perfect absorber with a graded nonlocal metamaterial. Appl. Phys. Lett. **114**(11), 101 (2019)

Xu, H., Liu, B., Zhang, H., Chen, Y.: Broadband and wide-angle terahertz absorber based on metasurface. Appl. Phys. Lett. **110**(14), 105 (2017)

Yang, J., Xiao, S., Yang, Z., Yang, Y., Qiu, C.: Flexible metamaterial absorbers with integrated filters for simultaneous electromagnetic wave absorption and harmonic generation. Adv. Mater. **25**(7), 328–332 (2013)

Zhao, Y., Zhang, B., Zhou, J., Huangfu, J., Chen, H.: Polarization-independent and wide-angle nearly perfect absorber with a phase transition material. Opt. Express **22**(14), 460–467 (2014)